Monthly Notices of the ROYAL ASTRONOMICAL SOCIETY

MNRAS **487,** 2947–2960 (2019) doi:10.1093/mnras/stz1453
Advance Access publication 2019 May 27

Merging black holes in young star clusters

Ugo N. Di Carlo,[1,2,3]★ Nicola Giacobbo,[2,3,4] Michela Mapelli,[2,3,4,5] Mario Pasquato,[2,3] Mario Spera,[2,3,4,5,6,7] Long Wang[8,9] and Francesco Haardt[1]

[1]*Dipartimento di Scienza e Alta Tecnologia, University of Insubria, Via Valleggio 11, I-22100 Como, Italy*
[2]*INAF-Osservatorio Astronomico di Padova, Vicolo dell'Osservatorio 5, I-35122 Padova, Italy*
[3]*INFN, Sezione di Padova, Via Marzolo 8, I-35131 Padova, Italy*
[4]*Dipartimento di Fisica e Astronomia 'G. Galilei', University of Padova, Vicolo dell'Osservatorio 3, I-35122 Padova, Italy*
[5]*Institut für Astro- und Teilchenphysik, Universität Innsbruck, Technikerstrasse 25/8, A-6020 Innsbruck, Austria*
[6]*Center for Interdisciplinary Exploration and Research in Astrophysics (CIERA), Evanston, IL 60208, USA*
[7]*Department of Physics & Astronomy, Northwestern University, Evanston, IL 60208, USA*
[8]*Argelander-Institut für Astronomie, Auf dem Hügel 71, D-53121 Bonn, Germany*
[9]*RIKEN Advanced Institute for Computational Science, 7-1-26 Minatojima-minami-machi, Chuo-ku, Kobe, Hyogo 650-0047, Japan*

Accepted 2019 May 22. Received 2019 May 16; in original form 2018 December 13

ABSTRACT

Searching for distinctive signatures, which characterize different formation channels of binary black holes (BBHs), is a crucial step towards the interpretation of current and future gravitational wave detections. Here, we investigate the demography of merging BBHs in young star clusters (SCs), which are the nursery of massive stars. We performed 4×10^3 *N*-body simulations of SCs with metallicity $Z = 0.002$, initial binary fraction 0.4, and fractal initial conditions, to mimic the clumpiness of star-forming regions. Our simulations include a novel population-synthesis approach based on the code MOBSE. We find that SC dynamics does not affect the merger rate significantly, but leaves a strong fingerprint on the properties of merging BBHs. More than 50 per cent of merging BBHs in young SCs form by dynamical exchanges in the first few Myr. Dynamically formed merging BBHs are significantly heavier than merging BBHs in isolated binaries: merging BBHs with total mass up to $\sim$120 $M_\odot$ form in young SCs, while the maximum total mass of merging BBHs in isolated binaries with the same metallicity is only $\sim$70 $M_\odot$. Merging BBHs born via dynamical exchanges tend to have smaller mass ratios than BBHs in isolated binaries. Furthermore, SC dynamics speeds up the merger: the delay time between star formation and coalescence is significantly shorter in young SCs. In our simulations, massive systems such as GW170729 form only via dynamical exchanges. Finally $\sim$2 per cent of merging BBHs in young SCs have mass in the pair-instability mass gap ($\sim$60–120 $M_\odot$). This represents a unique fingerprint of merging BBHs in SCs.

Key words: black hole physics – gravitational waves – methods: numerical – binaries: general – stars: kinematics and dynamics – galaxies: star clusters: general.

1 INTRODUCTION

The recent detection of gravitational waves (GWs; Abbott et al. 2016b) by LIGO (Aasi et al. 2015) and Virgo (Acernese et al. 2015) has opened up a new way to investigate the Universe. Out of the 11 GW events reported so far, 10 have been interpreted as the merger of two black holes (BHs; Abbott et al. 2016a,b,c, 2017a,b,f; The LIGO Scientific Collaboration & the Virgo Collaboration 2018a, b) and one as the merger of two neutron stars (NSs; Abbott et al. 2017c). The double NS merger was accompanied by electromagnetic emission almost in all the electromagnetic spectrum, from radio to gamma-rays (Abbott et al. 2017d,e; Alexander et al. 2017; Chornock et al. 2017; Coulter et al. 2017; Cowperthwaite et al. 2017; Goldstein et al. 2017; Margutti et al. 2017; Nicholl et al. 2017; Pian et al. 2017; Savchenko et al. 2017; Soares-Santos et al. 2017).

Seven out of 10 binary BH (BBH) mergers observed by the LIGO–Virgo collaboration harbour BHs with mass $\gtrsim 30\,M_\odot$, significantly higher than the range inferred from dynamical measurements of BH masses in nearby X-ray binaries (Orosz 2003; Özel et al. 2010; Farr et al. 2011). Such massive stellar BHs are expected to form from the direct collapse of massive metal-poor stars (e.g. Heger et al. 2003; Mapelli, Colpi & Zampieri 2009; Belczynski et al. 2010; Mapelli et al. 2010; Fryer et al. 2012; Mapelli et al. 2013;

★ E-mail: ugo_dc@hotmail.it

Spera, Mapelli & Bressan 2015; Spera & Mapelli 2017). Dynamical interactions in dense environments are also expected to significantly affect the mass spectrum of BHs (e.g. Portegies Zwart & McMillan 2000, 2002; Portegies Zwart et al. 2004; Gürkan, Fregeau & Rasio 2006; Giersz et al. 2015; Mapelli 2016). Alternatively, primordial BHs, which were predicted to form from gravitational instabilities in the very early Universe (Carr, Kühnel & Sandstad 2016; Raccanelli et al. 2016; Sasaki et al. 2016; Scelfo et al. 2018) might also have a mass of $\sim$30–40 $M_\odot$.

Not only the mass spectrum of compact objects but also the formation channels of compact-object binaries are matter of debate. Double compact objects might result from the evolution of isolated stellar binaries, i.e. systems of two stars which are gravitationally bound since their birth. An isolated binary (IB) is expected to undergo a number of processes during its life (including mass transfer, common envelope episodes, tidal forces, and supernova (SN) explosions). Binary population-synthesis codes are generally used to study the formation of double compact objects from the evolution of isolated stellar binaries (e.g. Tutukov & Yungelson 1973; Flannery & van den Heuvel 1975; Bethe & Brown 1998; Portegies Zwart & Yungelson 1998; Belczynski, Kalogera & Bulik 2002; Voss & Tauris 2003; Podsiadlowski et al. 2004, 2005; Belczynski et al. 2007, 2008; Moody & Sigurdsson 2009; Mennekens & Vanbeveren 2014; Tauris, Langer & Podsiadlowski 2015; Marchant et al. 2016; Tauris et al. 2017; Giacobbo, Mapelli & Spera 2018; Shao & Li 2018; Giacobbo & Mapelli 2019) and to estimate their merger rate density (e.g. Dominik et al. 2013, 2015; Belczynski et al. 2016a; de Mink & Mandel 2016; Mapelli et al. 2017; Chruslinska et al. 2018; Giacobbo & Mapelli 2018; Kruckow et al. 2018; Mapelli & Giacobbo 2018; Mapelli et al. 2018; Eldridge, Stanway & Tang 2019; Mapelli et al. 2019; Spera et al. 2019).

Alternatively, dynamics in dense environments, such as young star clusters (SCs), open clusters (Mapelli et al. 2013; Mapelli & Zampieri 2014; Ziosi et al. 2014; Kimpson et al. 2016; Mapelli 2016; Chatterjee et al. 2017; Kumamoto, Fujii & Tanikawa 2019; Rastello et al. 2019), globular clusters (Sigurdsson & Hernquist 1993; Sigurdsson & Phinney 1995; O'Leary et al. 2006; Sadowski et al. 2008; Downing et al. 2010, 2011; Rodriguez et al. 2015; Antonini & Rasio 2016; Hurley et al. 2016; O'Leary, Meiron & Kocsis 2016; Rodriguez, Chatterjee & Rasio 2016; Askar et al. 2017; Zevin et al. 2017; Antonini, Gieles & Gualandris 2019; Askar, Arca Sedda & Giersz 2018; Rodriguez et al. 2018; Samsing 2018), and nuclear SCs (Miller & Lauburg 2009; O'Leary, Kocsis & Loeb 2009; VanLandingham et al. 2016; Antonini et al. 2019; Arca-Sedda & Gualandris 2018; Hoang et al. 2018), can drive the formation and the evolution of compact-object binaries.

For example, dynamical exchanges can bring BHs into existing stellar binaries. BHs are particularly efficient in acquiring companions via exchanges, because they are among the most massive objects in an SC and exchanges tend to produce more and more massive binaries (Hills & Fullerton 1980). For this reason, Ziosi et al. (2014) find that $\gtrsim$ 90 per cent of BBHs in open clusters form via dynamical exchanges. Binaries formed through exchanges have a characteristic signature: they tend to be more massive than average, have high initial orbital eccentricity, and mostly misaligned spins.

Furthermore, dynamical hardening via three-body or multibody encounters can also affect the evolution of 'hard' binaries (i.e. binaries whose binding energy is higher than the average kinetic energy of other SC members, Heggie 1975), by shrinking their orbital separation until they enter the regime where GW emission proceeds efficiently (see e.g. Mapelli 2018 for a recent review). Finally, 'soft' binaries (i.e. binaries whose binding energy is lower than the average kinetic energy of other SC members) might even be broken by three-body and multibody encounters. Other dynamical processes which might affect the evolution of compact-object binaries include runaway collisions (e.g. Mapelli 2016), Spitzer's instability (Spitzer 1969), Kozai–Lidov resonances (Kozai 1962; Lidov 1962), and dynamical ejections (e.g. Downing et al. 2011). Three-body and multibody scattering experiments have shown that these effects are crucial for the demography of BBHs in SCs (Goodman & Hut 1993; Kulkarni, Hut & McMillan 1993; Miller & Hamilton 2002; Colpi, Mapelli & Possenti 2003; Antonini et al. 2016; Arca-Sedda, Li & Kocsis 2018; Samsing & D'Orazio 2018; Zevin et al. 2019).

Dynamics is a crucial ingredient to understand the formation of compact-object binaries because massive stars (which are thought to be the progenitors of BHs and NSs) form preferentially in young SCs and associations (Lada & Lada 2003; Portegies Zwart, McMillan & Gieles 2010). Thus, it is reasonable to expect that compact objects and their stellar progenitors participate in the dynamics of their parent SC, before being ejected or scattered into the field.

Despite this, most studies of BH dynamics neglect young SCs and star-forming regions, with few exceptions (Portegies Zwart & McMillan 2002; Banerjee, Baumgardt & Kroupa 2010; Kouwenhoven et al. 2010; Goswami, Kiel & Rasio 2014; Ziosi et al. 2014; Mapelli 2016; Banerjee 2017, 2018; Fujii, Tanikawa & Makino 2017; Kumamoto et al. 2019; Rastello et al. 2019). The relative scarcity of studies about BHs in young SCs is partially due to the fact that these are small, generally clumpy, and asymmetric stellar systems, mostly composed of few hundred to several thousand stars: they cannot be modelled with fast Monte Carlo techniques, but require expensive direct N-body simulations. Moreover, stellar evolution is a key ingredient in the life of young SCs, because their age is comparable with the lifetime of massive stars: mass-loss by stellar winds and SN explosions contribute significantly to the dynamical evolution of young stellar systems (e.g. Mapelli & Bressan 2013; Trani, Mapelli & Bressan 2014). This implies that dynamical models of young SCs should also include stellar evolution through accurate population synthesis.

Furthermore, observations suggest that young embedded SCs are characterized by clumpiness (e.g. Cartwright & Whitworth 2004; Gutermuth et al. 2005) and high fractions of binaries (e.g. Sana et al. 2012), whereas most simulations of young SCs adopt idealized initial conditions, consisting of monolithic King models (King 1966) and assuming a very small fraction of binaries ($f \sim$ 0–0.1).

Our aim is to study the demography of double compact objects in young SCs, following a novel approach: we have run a large set of N-body simulations of young SCs with fractal initial conditions (which mimic the clumpy and asymmetric structure of star-forming regions, e.g. Goodwin & Whitworth 2004) and with a high initial binary fraction ($f_{\rm bin} = 0.4$). The initial masses of our SCs have been randomly drawn according to a power-law distribution $\mathrm{d}N/\mathrm{d}M_{\rm SC} \propto M_{\rm SC}^{-2}$ (from $M_{\rm SC} = 10^3$ $M_\odot$ to 3×10^4 $M_\odot$), consistent with the mass distribution of young SCs in the Milky Way (Elmegreen & Efremov 1997; Lada & Lada 2003). While these SCs host fewer stars than globular clusters and other massive clusters, they make up the vast majority of the SCs in the Universe (Kroupa & Boily 2002), and their cumulative contribution to BH statistics may thus be significant. We evolve each SC with an accurate treatment of dynamics (Wang et al. 2015) and with up to date binary population-synthesis models (Giacobbo et al. 2018).

2 METHODS

The simulations were done using the direct summation *N*-body code NBODY6++ GPU (Wang et al. 2015) coupled with the new population synthesis code MOBSE (Giacobbo et al. 2018).

2.1 Direct *N*-body

NBODY6++ GPU is the GPU parallel version of NBODY6 (Aarseth 2003). It implements a fourth-order Hermite integrator, individual block time-steps (Makino & Aarseth 1992), and Kustaanheimo–Stiefel (KS) regularization of close encounters and few-body subsystems (Stiefel 1965).

A neighbour scheme (Nitadori & Aarseth 2012) is used to compute the force contributions at short time intervals (*irregular* force/time-steps), while at longer time intervals (*regular* force/time-steps) all the members in the system contribute to the force evaluation. The irregular forces are evaluated using CPUs, while the regular forces are computed on GPUs using the CUDA architecture. This version of NBODY6++ GPU does not include post-Newtonian terms.[1]

2.2 Population synthesis

In its original version, NBODY6++ GPU is coupled with the population synthesis code BSE (Hurley, Pols & Tout 2000; Hurley, Tout & Pols 2002). For this work, we modified NBODY6++ GPU, coupling it with the new population synthesis code MOBSE (Mapelli et al. 2017; Giacobbo et al. 2018; Giacobbo & Mapelli 2018, 2019; Mapelli & Giacobbo 2018), an updated version of BSE. NBODY6++ GPU and MOBSE are perfectly integrated: they update stellar parameters and trajectories simultaneously during the computation.

MOBSE implements some of the most recent stellar wind models for massive hot stars (Vink, de Koter & Lamers 2001; Gräfener & Hamann 2008; Vink et al. 2011; Vink 2016), including the impact of the Eddington factor Γ_e on mass-loss (Gräfener & Hamann 2008; Chen et al. 2015). Here, we adopt the following definition of Γ_e:

$$\log \Gamma_e = -4.813 + \log(1 + X_H) + \log(L/L_\odot) - \log(M/M_\odot), \quad (1)$$

where X_H is the Hydrogen fraction, L is the stellar luminosity, and M is the stellar mass.

In MOBSE the mass-loss of massive hot stars (O- and B-type main-sequence stars, luminous blue variable stars, and Wolf–Rayet stars) scales as $\dot{M} \propto Z^\beta$, where β is defined as (Giacobbo & Mapelli 2018)

$$\beta = \begin{cases} 0.85 & \text{if} \quad \Gamma_e < 2/3 \\ 2.45 - 2.4\Gamma_e & \text{if} \quad 2/3 \leq \Gamma_e < 1 \\ 0.05 & \text{if} \quad \Gamma_e \geq 1 \end{cases} . \quad (2)$$

MOBSE includes two different prescriptions for core-collapse supernovae (SNe) from Fryer et al. (2012): the *rapid* and the *delayed* SN models. The former model assumes that the SN explosion only occurs if it is launched $\lesssim 250$ ms after the bounce, while the latter has a longer time-scale ($\gtrsim 500$ ms). In both models, a star is assumed to directly collapse into a BH if its final carbon–oxygen mass is $\gtrsim 11\ M_\odot$. For the simulations described in this paper we adopt the *delayed* model. Recipes for electron-capture SNe are also included in MOBSE (Hurley et al. 2000; Fryer et al. 2012; Giacobbo & Mapelli 2019).

Prescriptions for pair-instability SNe (PISNe) and pulsational pair-instability SNe (PPISNe) are implemented using the fitting formulas by Spera & Mapelli (2017). In particular, stars which grow a Helium core mass $64 \leq m_{He}/M_\odot \leq 135$ are completely disrupted by a PISN and leave no compact object, while stars with $32 \leq m_{He}/M_\odot < 64$ undergo a PPISN: they evolve through a set of pulsations, which enhance mass-loss and cause the final remnant mass to be significantly smaller than they would be if we had accounted only for core-collapse SNe. According to our current knowledge of PISNe and PPISNe and to the stellar evolution prescriptions implemented in MOBSE, we expect no compact objects in the mass range $\sim$60–120 $M_\odot$ from single stellar evolution. Binary evolution might affect this range. For example, mass accretion on to an evolved star (or the merger between a post-main-sequence star and a main-sequence star) might increase the mass of the Hydrogen envelope without significantly affecting the Helium core: at the time of collapse, such star will have a Helium core mass below the PPISN/PISN range, but a significantly larger Hydrogen envelope. By direct collapse, this star might produce a BH with mass $\geq$60 $M_\odot$. Clearly, the possibility of forming BHs with mass in the PPISN/PISN gap depends on the assumptions about efficiency of mass accretion, about mass-loss after stellar mergers, and about core-collapse SNe.

Due to these assumptions for massive star evolution and SNe, the BH mass spectrum predicted by MOBSE depends on progenitor's metallicity (the maximum BH mass being higher at lower metallicity) and is consistent with LIGO–Virgo detections[2] (Abbott et al. 2016a,b,c, 2017a,b,f; The LIGO Scientific Collaboration & the Virgo Collaboration 2018a).

Natal kicks are randomly drawn from a Maxwellian velocity distribution. A one-dimensional root mean square velocity $\sigma_{CCSN} = 265$ km s^{-1} and $\sigma_{ECSN} = 15$ km s^{-1} are adopted for core-collapse SNe (Hobbs et al. 2005) and for electron-capture SNe (Dessart et al. 2006; Jones et al. 2013; Schwab, Quataert & Bildsten 2015; Giacobbo & Mapelli 2019), respectively. Kick velocities of BHs are reduced by the amount of fallback as $V_{KICK} = (1 - f_{fb})\,V$, where f_{fb} is the fallback parameter described in Fryer et al. (2012) and V is the velocity drawn from the Maxwellian distribution.

Binary evolution processes such as tidal evolution, Roche lobe overflow, common envelope, and GW energy loss are taken into account as described in Hurley et al. (2002). In particular, our treatment of common envelope depends on two parameters: α (describing the efficiency of energy transfer) and λ (describing the geometry of the envelope and the importance of recombinations). In this work, we assume $\alpha = 3$, while λ is derived by MOBSE as described in Claeys et al. (2014).

Orbital decay and circularization by GW emission are calculated according to Peters (1964) without explicitly including post-Newtonian terms. The standard version of BSE calculates GW energy loss only if the two binary members are closer than 10

[1] In other versions of NBODY, general relativity is taken into account in the algorithmic regularization routine via post-Newtonian terms. As recently discussed in several works (Samsing, MacLeod & Ramirez-Ruiz 2017; Arca-Sedda et al. 2018; Rodriguez et al. 2018; Samsing, Askar & Giersz 2018; Zevin et al. 2019), including post-Newtonian terms in *N*-body simulations might increase the chance for BBHs to merge inside the cluster before ejection, thus increasing the total number of merging events.

[2] The BHs detected thus far by LIGO and Virgo are consistent with a power-law mass distribution with index $1.6^{+1.5}_{-1.7}$ (at 90 per cent credibility) and with maximum mass $\sim$45 $M_\odot$ (e.g. The LIGO Scientific Collaboration & The Virgo Collaboration 2018b).

$R_\odot$, which has been shown to lead to a serious underestimation of the merger rate of eccentric binaries in dynamical simulations (Samsing 2018). In MOBSE, we remove the 10 $R_\odot$ limit: GW decay is calculated for all binaries of two compact objects (white dwarfs, NSs, and BHs).

Finally, if two stars merge during the *N*-body simulations, the amount of mass-loss is decided by MOBSE, which adopts the same prescriptions as BSE, but for one exception: if a star merges with a BH or an NS, MOBSE assumes that the entire mass of the star is immediately lost by the system and the BH (or NS) does not accrete it (while the version of BSE implemented in NBODY6++GPU assumes that the entire mass is absorbed by the compact object). This assumption by MOBSE is very conservative, because it is highly unlikely that the compact object can accrete a substantial fraction of the stellar mass, but it is hard to quantify the actual mass accretion.

2.3 Initial conditions

We generate the initial conditions with MCLUSTER (Küpper et al. 2011), which allows to produce models with different degrees of fractal substructures (Goodwin & Whitworth 2004). The level of fractality is decided by the parameter D (where $D = 3$ means homogeneous distribution of stars). In this work, we adopt $D = 1.6$ (high-fractality runs[3]) and $D = 2.3$ (low-fractality runs). The qualitative difference between these two fractal dimensions is represented in Fig. 1.

In this work, we have simulated 4×10^3 fractal young SCs: half of them with $D = 1.6$ (HF sample) and the remaining half with $D = 2.3$ (LF sample). The total mass $M_{\rm SC}$ of each SC (ranging from 1000 to 30000 $M_\odot$) is drawn from a distribution $dN/dM_{\rm SC} \propto M_{\rm SC}^{-2}$, as the embedded SC mass function described in Lada & Lada (2003). Thus, the mass distribution of our simulated SCs mimics the mass distribution of SCs in Milky Way-like galaxies. We choose the initial SC half-mass radius $r_{\rm h}$ according to the Marks and Kroupa relation (Marks et al. 2012), which relates the total mass $M_{\rm SC}$ of an SC at birth with its initial half-mass radius $r_{\rm h}$:

$$r_h = 0.10^{+0.07}_{-0.04}\,{\rm pc}\left(\frac{M_{\rm SC}}{M_\odot}\right)^{0.13\pm0.04}. \quad (3)$$

The SCs are initialized in virial equilibrium.

All simulated SCs have stellar metallicity $Z = 0.002$, i.e. 1/10 of the solar metallicity (if we assume solar metallicity $Z_\odot = 0.02$). The stars in the simulated SCs follow a Kroupa (2001) initial mass function, with minimum mass 0.1 $M_\odot$ and maximum mass 150 $M_\odot$.

We assume an initial binary fraction $f_{\rm bin} = 0.4$. The orbital periods, eccentricities, and mass ratios of binaries are drawn from Sana et al. (2012). In particular, we obtain the mass of the secondary m_2 as follows:

$$\mathfrak{F}(q) \propto q^{-0.1} \qquad \text{with} \quad q = \frac{m_2}{m_1} \in [0.1 - 1], \quad (4)$$

the orbital period P from

$$\mathfrak{F}(\mathscr{P}) \propto (\mathscr{P})^{-0.55} \quad \text{with } \mathscr{P} = \log_{10}(P/{\rm d}) \in [0.15\text{–}5.5] \quad (5)$$

and the eccentricity e from

$$\mathfrak{F}(e) \propto e^{-0.42} \qquad \text{with} \quad 0 \le e < 1. \quad (6)$$

[3]Portegies Zwart (2016) suggest that the fractal dimension of young SCs should be ∼1.6 by comparing observations of the Orion Trapezium Cluster with *N*-body simulations.

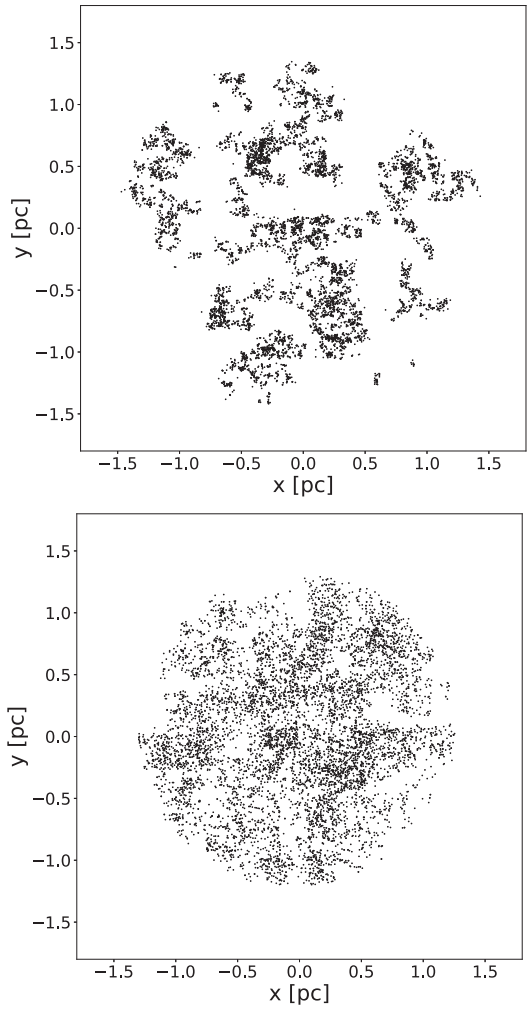

Figure 1. SC models generated with the MCLUSTER code. Each point represents a star. Both SCs have a total mass of 5000 $M_\odot$. Top: model with fractal dimension $D = 1.6$. Bottom: model with fractal dimension $D = 2.3$.

In a forthcoming paper we will also investigate the effects of different metallicities, virial ratios, and initial binary fractions.

The force integration includes a solar neighbourhood-like static external tidal field. In particular, the potential is point-like and the simulated SCs are assumed to be on a circular orbit around the centre of the Milky Way with a semimajor axis of 8 kpc (Wang et al. 2016). Each SC is evolved until its dissolution or for a maximum time $t = 100$ Myr. The choice of terminating the simulations at $t = 100$ Myr is motivated by the fact that our tidal field model tends to overestimate the lifetime of SCs because we do not account for massive perturbers (e.g. molecular clouds), which accelerate the SC disruption (Gieles et al. 2006).

We compare the results of the SC simulations with IB simulations performed with the standalone version of MOBSE. In particular, we simulate 10^7 IBs with the same initial conditions as SC binaries, i.e. metallicity $Z = 0.002$, primary mass drawn from a Kroupa (Kroupa 2001) mass function between 0.1 and 150 $M_\odot$, secondary mass, eccentricity, and orbital periods derived from Sana et al. (2012).

A summary of the initial conditions of the performed simulations is reported in Table 1. In the following, we consider four simulation sets: (i) HF: simulated SCs with high level of fractality ($D = 1.6$);

Table 1. Initial conditions.

Set	Run number	$M_{\rm SC}$ ($M_\odot$)	$r_{\rm h}$ (pc)	Z	$f_{\rm bin}$	D	IMF	$m_{\rm min}$ ($M_\odot$)	$m_{\rm max}$ ($M_\odot$)
HF	2×10^3	$10^3 - 3 \times 10^4$	$0.1 \times (M_{\rm SC}/M_\odot)^{0.13}$	0.002	0.4	1.6	Kroupa (2001)	0.1	150
LF	2×10^3	$10^3 - 3 \times 10^4$	$0.1 \times (M_{\rm SC}/M_\odot)^{0.13}$	0.002	0.4	2.3	Kroupa (2001)	0.1	150
SC	4×10^3	$10^3 - 3 \times 10^4$	$0.1 \times (M_{\rm SC}/M_\odot)^{0.13}$	0.002	0.4	1.6, 2.3	Kroupa (2001)	0.1	150
IB	10^7	–	–	0.002	1.0	–	Kroupa (2001)	5	150

Note: Column 1: Name of the simulation set. HF: high fractality ($D = 1.6$) N-body simulations; LF: low fractality ($D = 2.3$) N-body simulations; SC: all N-body simulations considered together (i.e. set HF + set LF); IB: isolated binaries (population synthesis simulations run with MOBSE, without dynamics). Column 2: Number of runs; column 3: total mass of SCs ($M_{\rm SC}$); column 4: half-mass radius ($r_{\rm h}$); column 5: metallicity (Z); column 6: initial binary fraction ($f_{\rm bin}$); column 7: fractal dimension (D); column 8: initial mass function (IMF); column 9: minimum mass of stars ($m_{\rm min}$); column 10: maximum mass of stars ($m_{\rm max}$).

(ii) LF: simulated SCs with low level of fractality ($D = 2.3$); (iii) SC: all simulated SCs (considering HF and LF simulations together); (iv) IB: isolated binary simulations run with the standalone version of MOBSE.

3 RESULTS

3.1 Statistics of dynamically formed double BHs (BBHs)

First, we estimate how many BBHs form via dynamical channels in our simulations. We define *exchanged binaries* as binaries formed via dynamical exchanges, whereas those binaries which were generated in the initial conditions are dubbed as *original binaries*.[4] At the end of the simulations ($t = 100$ Myr), ∼85–89 per cent of all surviving BBHs are exchanged binaries. Thus, dynamical exchanges give an important contribution to the population of BBHs. We find no significant differences between runs with high fractal number (HF) and with low fractal number (LF). Table 2 shows the statistics for the different simulation sets.

We check how many of these BBHs are expected to merge by GW decay within a Hubble time ($t_{\rm H} = 14$ Gyr). No binaries merge during the dynamical simulations. Thus, to calculate the merging time, we use the following equation (Peters 1964)

$$t_{\rm GW} = \frac{5}{256} \frac{c^5\, a^4\, (1-e^2)^{7/2}}{G^3\, m_1\, m_2\, (m_1+m_2)}, \quad (7)$$

where c is the speed of light, G is the gravitational constant, e is the eccentricity of the binary, a is the semimajor axis of the binary, m_1 and m_2 are the masses of the primary and of the secondary BH, respectively. For each binary, we take the values of a and e at the end of the simulation (during the simulation, MOBSE integrates the change of eccentricity and semimajor axis driven by GW decay using a similar formalism, derived from Peters 1964).

The number of BBHs merging within a Hubble time (hereafter, merging BBHs) is also shown in Table 2. More than half of merging BBHs (∼50 per cent and ∼56 per cent in HF and LF simulations, respectively) are exchanged binaries, confirming the importance of dynamical exchanges for merging BBHs. Moreover, only four merging BBHs ($\lesssim 2$ per cent of all merging BBHs) are still members of their parent SC at the end of the simulation, while the others have all been dynamically ejected.

These results confirm the importance of dynamics, and in particular of dynamical exchanges, for the demography of BBHs in small young SCs. Interestingly, the vast majority (if not all) of dynamically formed merging BBHs are no longer members of their parent SC when they merge, because of dynamical ejections.

Overall, the populations of merging BBHs in HF and LF simulations show a similar trend. For this reason, in the rest of the paper, we will consider HF and LF simulations as a single simulation set (SC simulations), unless otherwise specified. We will discuss the differences between HF and LF simulations in Section 3.6.

3.2 BH mass distribution

The next step is to understand whether BBHs formed in young SCs have distinctive features with respect to IBs. In this section, we consider the mass of BHs.

3.2.1 *BH mass versus ZAMS mass*

Fig. 2 shows the mass of all simulated BHs with mass $m_{\rm BH} < 150\ M_\odot$ (both single and binary BHs) as a function of the zero-age main sequence (ZAMS) mass of the progenitor star. The left-hand panel shows the results of the SC simulations (considering BBHs from models HF and LF together, because the level of fractality does not significantly affect the masses, see Table 3), while the right-hand panel shows the comparison sample of IBs. The BH mass we obtain from the evolution of single stars is shown as a red dotted line in both plots.

Dynamics does not affect significantly the mass of the majority of BHs: the most densely populated regions of the plot are the same in both panels. Binary evolution processes (especially mass transfer and common envelope) have a much stronger impact than dynamics on the mass of most BHs. For example, the large number of BHs with mass higher than expected from single star evolution (red dotted line) for progenitors with ZAMS mass $M_{\rm ZAMS} < 60\ M_\odot$ is an effect of mass accretion, while most of the BHs with mass lower than expected from single star evolution originate from donor stars whose envelope was peeled off (see Giacobbo & Mapelli 2018 and Spera et al. 2019 for more details on the effects of binary evolution on BH masses).

However, dynamics crucially affects the maximum mass of BHs (see also Fig. 3). In the N-body simulations, BHs with mass up to ∼440 $M_\odot$ are allowed to form, while the maximum mass of BHs formed from IB evolution is ∼60 $M_\odot$. In Figs 2 and 3, we show only BHs with mass $<150\ M_\odot$ for clarity. BHs with mass $>150\ M_\odot$ are very rare and including them would make these figures more difficult to read. Fig. 4 shows the BHs with mass $m_{\rm BH} \geq 150\ M_\odot$. These are intermediate-mass BHs (IMBHs) formed by runaway collisions of stars in the early evolution of the SC (see e.g. Portegies Zwart & McMillan 2002; Portegies Zwart et al. 2004; Giersz et al.

[4] Usually, dynamicists use the adjective *primordial* to refer to binaries which are already present in the initial conditions, but we use a different adjective to avoid confusion with primordial BHs (i.e. BHs which originate from gravitational instabilities in the early Universe Carr et al. 2016).

Table 2. Number of SC BBHs.

Set	Exchanged BBHs	Original BBHs	Merging exchanged BBHs	Merging original BBHs
HF	710	124	60	59
LF	786	98	62	48

Note: Number of BBHs in HF and LF simulations. Column 1: Name of the simulation set; column 2: number of BBHs that formed from dynamical exchanges and that are still bound at the end of the simulations ($t = 100$ Myr); column 3: number of BBHs that formed from original binaries and that are still bound at the end of the simulations ($t = 100$ Myr); column 4: number of BBHs that formed from dynamical exchanges and that merge within a Hubble time (hereafter merging exchanged BBHs); column 5: number of BBHs that formed from original binaries and that merge within a Hubble time (hereafter merging original BBHs).

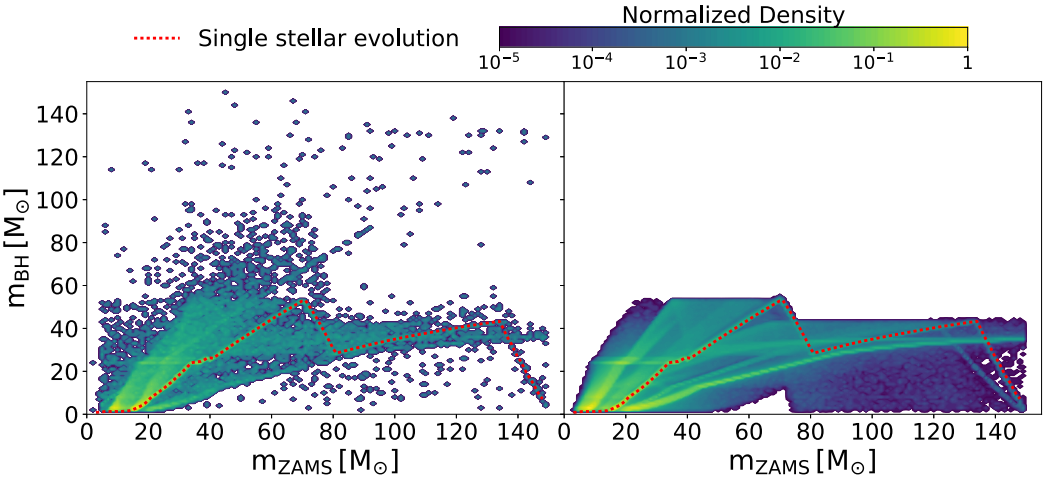

Figure 2. BH mass (m_{BH}) as a function of the zero-age main sequence (ZAMS) mass of the progenitor stars (m_{ZAMS}) in the SC simulations (left), and in IBs evolved with MOBSE (right). The logarithmic colour bar represents the number of BHs per cell, normalized to the maximum cell value of each plot. Each cell is a square with a side of 1.5 $M_\odot$. The red dashed line represents the mass spectrum of compact objects obtained from single stellar evolution. Dynamical interactions trigger the formation of more massive BHs. Intermediate-mass BHs (IMBHs, i.e. BHs with mass $m_{BH} > 150$ $M_\odot$) and second-generation BHs (Gerosa & Berti 2017, i.e. the products of the merger of two BHs) are not shown in this Figure.

Table 3. Results of the U-Test and KS-Test to compare two BBH samples.

BBH sample 1	BBH sample 2	Distribution	U-Test	KS-Test	Median 1	Median 2
HF – Merging BBHs	LF – Merging BBHs	m_{tot}	0.57	0.20	32.8 $M_\odot$	35.4 $M_\odot$
HF – Merging BBHs	LF – Merging BBHs	m_{chirp}	0.51	0.50	14.0 $M_\odot$	14.6 $M_\odot$
HF – Merging BBHs	LF – Merging BBHs	q	0.03	0.05	0.88	0.81
HF – Merging BBHs	LF – Merging BBHs	t_{exch}	0.04	0.11	1.9 Myr	2.8 Myr
SC – Merging BBHs	IB – Merging BBHs	m_{tot}	0	0	34.7 $M_\odot$	24.0 $M_\odot$
SC – Merging BBHs	IB – Merging BBHs	m_{chirp}	0	0	14.2 $M_\odot$	10.4 $M_\odot$
SC – Merging BBHs	IB – Merging BBHs	q	10^{-7}	10^{-7}	0.84	0.89
SC – Merging Exchanged BBHs	SC – Merging Original BBHs	m_{tot}	10^{-8}	10^{-8}	41.5 $M_\odot$	30.2 $M_\odot$
SC – Merging Exchanged BBHs	IB – Merging BBHs	m_{tot}	0	0	41.5 $M_\odot$	24.0 $M_\odot$
SC – Merging Original BBHs	IB – Merging BBHs	m_{tot}	10^{-9}	10^{-9}	30.2 $M_\odot$	24.0 $M_\odot$
SC – Merging Exchanged BBHs	SC – Merging Original BBHs	m_{chirp}	10^{-5}	10^{-7}	16.9 $M_\odot$	13.2 $M_\odot$
SC – Merging Exchanged BBHs	IB – Merging BBHs	m_{chirp}	0	0	16.9 $M_\odot$	10.4 $M_\odot$
SC – Merging Original BBHs	IB – Merging BBHs	m_{chirp}	10^{-9}	10^{-9}	13.2 $M_\odot$	10.4 $M_\odot$
SC – Merging Exchanged BBHs	SC – Merging Original BBHs	q	10^{-4}	10^{-4}	0.78	0.89
SC – Merging Exchanged BBHs	IB – Merging BBHs	q	10^{-9}	10^{-9}	0.78	0.89
SC – Merging Original BBHs	IB – Merging BBHs	q	0.27	0.14	0.89	0.89

Note: In this Table we apply the U- and KS- tests to compare different samples of merging BBHs (i.e. BBHs merging within a Hubble time). Columns 1 and 2: the two BBH samples to which we apply the U- and KS- test. Each sample comes from one of the simulation sets (HF, LF, SC, and IB, see Table 1). For the SC sample we also distinguish between 'Exchanged BBHs' and 'Original BBHs' (see Section 3.1 for the definition). Column 3: distribution to which we apply the U- and KS- tests. We consider total BBH masses (m_{tot}), chirp masses (m_{chirp}), mass ratios (q), and time of the exchange (t_{exch}, for exchanged binaries only). Columns 4 and 5: probability that the two samples are drawn from the same distribution according to the U-Test and to the Kolmogorov–Smirnov (KS) Test, respectively. Values smaller than 10^{-20} are indicated with 0. Columns 6 and 7: median values of the distributions of BBH sample 1 and 2, respectively.

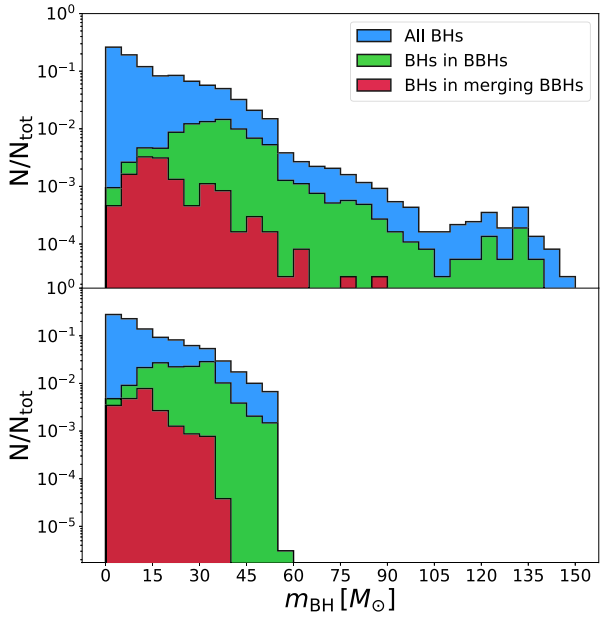

Figure 3. Top (Bottom) panel: distribution of BH masses in the SC (IB) simulations. Blue: all BHs excluding IMBHs and second-generation BHs; green: BHs which reside in BBH systems at the end of the simulations; red: BHs in merging BBH systems.

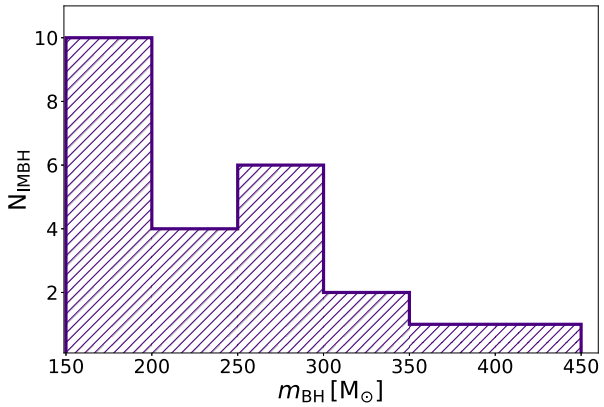

Figure 4. Mass distribution of the 24 IMBHs formed by runaway collisions in our SC simulations.

2015; Mapelli 2016). In our simulations, we find 24 IMBHs, which represent only the 0.065 per cent of all simulated BHs.

The percentage of BHs with mass >70 $M_\odot$ in the *N*-body simulations is only $\sim$1 per cent of all BHs ($\sim$0.92 per cent and $\sim$0.96 per cent in LF and HF simulations, respectively). Thus, they are very rare, but their large mass is a clear signature of dynamical origin. These massive BHs form because of multiple stellar mergers, which can happen only in SCs. In fact, if the two members of an IB merge together, the probability that their merger product acquires a new companion is negligible; whereas the merger product of a binary in an SC has a good chance to acquire a new companion dynamically (especially if it is particularly massive) and might merge also with new companion (Mapelli 2016). Of course, these multiple mergers are mostly mergers of stars, because mergers of BBHs are much rarer events (see next section). In particular, the most massive BHs in our simulations form from the merger of at least four stars.

Because the most massive BHs originate from multiple stellar mergers (or even runaway collisions), the maximum BH mass in the *N*-body simulations essentially does not depend on the ZAMS mass of the progenitor (in the case of mergers, Fig. 2 shows the ZAMS mass of the most massive among the stellar progenitors).

We expect PISNe and PPISNe to prevent the formation of BHs with mass $\sim$60–120 $M_\odot$ from single stellar evolution (Belczynski et al. 2016b; Spera & Mapelli 2017; Woosley 2017). On the other hand, Spera et al. (2019) have already shown that binary evolution might produce few BHs in the mass gap. For example, the merger between an evolved star (with an already well developed Helium or Carbon–Oxygen core) and a main-sequence star might produce a very massive star with a large Hydrogen envelope but with a Helium core smaller than required to enter the pair-instability range. Such star might end its life directly collapsing to a BH with mass in the pair-instability gap. In an SC, such massive BHs have additional chances to form (see e.g. Mapelli 2016), because multiple mergers between stars are likely.

Moreover, if a BH with mass $\sim$60–120 $M_\odot$ forms from the merger of an IB, it will remain a single BH. In contrast, if a BH with mass 60–120 $M_\odot$ forms from a binary in an SC, it might acquire another companion by dynamical exchange and merge via GW emission (see Section 3.2.3 for more details on these systems).

3.2.2 *Mass of single versus binary BHs*

The top panel of Fig. 3 compares the mass distribution of all BHs with $m_{\rm BH} < 150$ $M_\odot$ formed in the *N*-body simulations (including merger products) with the mass of BHs which are members of BBHs by the end of the *N*-body simulations. Light BHs are less likely to be members of a binary than massive BHs: just $\sim$4 per cent of BHs with mass lower than 30 $M_\odot$ reside in BBHs by the end of the SC simulations, while $\sim$29 per cent of BHs with mass larger than 30 $M_\odot$ have a BH companion by the end of the SC simulations.

The bottom panel of Fig. 3 shows the same quantities for the IB simulations. The difference between top and bottom panel is apparent: no BHs with mass larger than 60 $M_\odot$ form in the IB simulations at metallicity $Z = 0.002$, while SC dynamics induces the formation of BHs with mass up to $\sim$440 $M_\odot$ (Fig. 4).

We stress that BHs with mass $\gtrsim 60$ $M_\odot$ are inside the mass gap expected from PISNe and PPISNe (Belczynski et al. 2016a; Spera & Mapelli 2017; Woosley 2017): they can form dynamically because of multiple mergers between stars.

3.2.3 *Mass of merging BHs: exchanged, original, and isolated binaries*

From Fig. 3 it is apparent that the most massive BHs do not merge within a Hubble time, in both IBs and SCs. This effect was already discussed in previous work (Giacobbo et al. 2018; Giacobbo & Mapelli 2018; Spera et al. 2019) and is a consequence of the stellar radius evolution of the progenitors of such massive BHs.[5]

[5]Unless chemical homogeneous evolution is assumed, the radii of massive stars ($m_{\rm ZAMS} \gtrsim 40$ $M_\odot$) reach values of several hundred to several thousand $R_\odot$. Stellar binaries with initial orbital separation larger than these radii survive early coalescence and can evolve into massive BBHs, but the latter cannot merge via GW decay because their semimajor axis is too large. In contrast, stellar binaries with smaller orbital separations either merge before becoming BHs or undergo a non-conservative mass transfer (or common envelope) process. At the end of this process, the binary might survive and

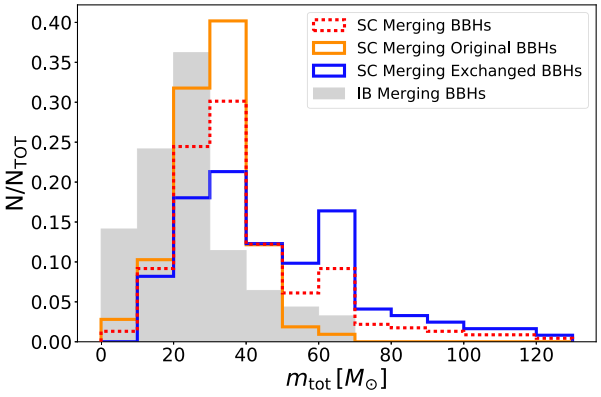

Figure 5. Distribution of total masses ($m_{\rm tot} = m_1 + m_2$) of merging BBHs. Orange solid line: original BBHs formed in SCs; blue solid line: exchanged BBHs formed in SCs; red dashed line: all merging BBHs formed in SCs (original + exchanged); grey filled histogram: BBHs formed in isolated binaries (IBs). Each distribution is normalized to its total number of elements.

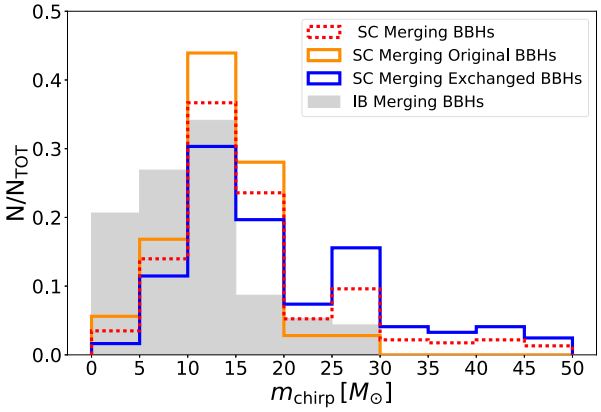

Figure 6. Same as Fig. 5, but for the distribution of chirp masses $m_{\rm chirp} = (m_1\,m_2)^{3/5}(m_1+m_2)^{-1/5}$ of merging BBHs.

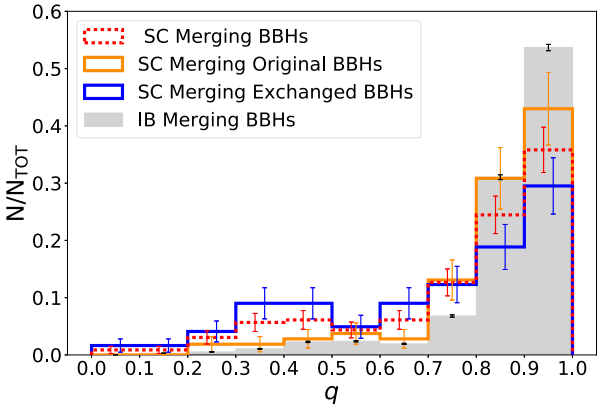

Figure 7. Same as Fig. 5, but for the distribution of mass ratios $q = m_2/m_1$ of merging BBHs. The error bars represent Poisson uncertainties.

If we compare the two red histograms in the top and bottom panel, we see that the maximum mass of merging BHs is larger in SCs than in IBs. Thus, dynamics triggers the merger of some massive (>40 $M_\odot$) BHs, which cannot merge if they evolve in IBs.

Fig. 5 shows the total masses ($m_{\rm tot} = m_1 + m_2$) of merging exchanged and original BBHs in SCs. The former are merging BBHs which form from exchanged binaries in SC simulations, while the latter are merging BBHs which form from original binaries in SC simulations. For comparison, we also show the total masses of merging BBHs from IB simulations. The distribution of exchanged BBHs is markedly different from the other two. In particular, merging exchanged BBHs tend to be more massive than original BBHs: $m_{\rm tot} \leq 70$ $M_\odot$ for both isolated BBHs and original BBHs, while merging exchanged BBHs can reach $m_{\rm tot} \sim 120$ $M_\odot$. Table 3 shows the results of the Wilcoxon U-test (Bauer 1972; Hollander & Wolfe 1999) and of the Kolmogorov–Smirnov (KS) test (Birnbaum & Tingey 1951; Wang, Tsang & Marsaglia 2003), which confirm that the mass distribution of merging exchanged BBHs is not consistent with the other two classes of merging BBHs.

This large difference can be easily explained with the properties of dynamical exchanges: exchanges tend to favour the formation of more and more massive binaries because these are more energetically stable (see e.g. Hills & Fullerton 1980).

Interestingly, the mass distribution of merging original BBHs is also significantly different from the distribution of merging BBHs formed from IB simulations (see Table 3). Since both IBs and original binaries in SCs were evolved with the same population synthesis code (MOBSE), dynamical effects are the only way to explain this difference. Even if they do not form through dynamical exchanges, also original BBHs participate in the dynamical life of an SC: they can be hardened or softened or even ionized by three-body encounters. More massive BBHs are more likely to be hardened by three-body encounters, while light BBHs are more likely to be softened or ionized. This explains why merging original BBHs tend to be more massive than merging BBHs in IBs. Thus, dynamics affects almost the entire population of merging BBHs in SCs: not only exchanged BBHs, but also original BBHs.

Similar considerations apply also to the distribution of chirp masses $m_{\rm chirp} = (m_1\,m_2)^{3/5}(m_1+m_2)^{-1/5}$ (Fig. 6): we find no merging original BBHs with $m_{\rm chirp} > 30$ $M_\odot$, while merging exchanged BBHs reach $m_{\rm chirp} \sim 50$ $M_\odot$.

Fig. 7 shows the mass ratios of merging BBHs (defined as $q = m_2/m_1$). All distributions peak at $q \sim 1$. However, small mass ratios are significantly more likely in merging exchanged BBHs than in both merging original and isolated BBHs. Moreover, merging exchanged BBHs show a (marginally statistically significant) bump around $q \sim 0.4$. Table 3 confirms that the distribution of q of the merging exchanged BBHs is significantly different from both merging original BBHs and IBs. This can be easily explained with the different formation channels. If two BHs form from the same close stellar binary, mass transfer and common envelope episodes tend to 'redistribute' the mass inside the system, leading to the formation of two BHs with similar mass. In contrast, if two BHs enter the same binary by exchange, after they are formed, their mass cannot change anymore and even extreme mass ratios $q \sim 0.1$ are possible.

Finally, Fig. 8 shows the mass of the primary BH versus the mass of the secondary BH of merging systems. The first 10 GW events associated with BBHs are also shown. It must be kept in mind that we are not weighing the simulated distributions for the probability of observing them with LIGO–Virgo (e.g. more massive BHs can be

evolve into a BBH, but the mass of the two BHs will be significantly smaller than expected from single stellar evolution, because of mass-loss during mass transfer (Giacobbo & Mapelli 2018; Spera et al. 2019).

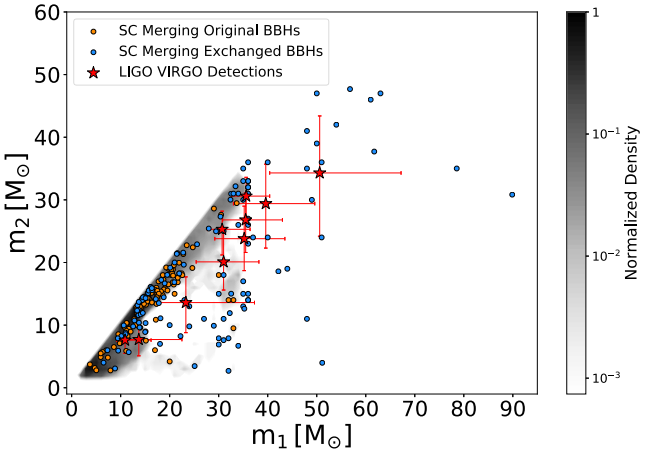

Figure 8. Mass of the primary BH (m_1) versus mass of the secondary BH (m_2) of merging BBHs. Filled contours (with grey colour map): IBs; orange circles: SC merging original BBHs; blue circles: SC merging exchanged BBHs; red stars with error bars: LIGO–Virgo detections of BH mergers – GW150914 (Abbott et al. 2016b), GW151012 (Abbott et al. 2016a), GW151226 (Abbott et al. 2016c), GW170104 (Abbott et al. 2017a), GW170608 (Abbott et al. 2017f), GW170729 (The LIGO Scientific Collaboration & the Virgo Collaboration 2018a), GW170809 (The LIGO Scientific Collaboration & the Virgo Collaboration 2018a), GW170814 (Abbott et al. 2017b), GW170818 (The LIGO Scientific Collaboration & the Virgo Collaboration 2018a), and GW170823 (The LIGO Scientific Collaboration & the Virgo Collaboration 2018a). Error bars indicate 90 per cent credible levels.

observed to a farther distance than light BHs, Abbott et al. 2016d). From this Figure, it is apparent that the LIGO–Virgo BBHs lie in a region of the $m_1 - m_2$ plane which is well populated by both IB and SC merging BBHs at metallicity $Z = 0.002$. Merging exchanged BHs are clearly different from the other two populations, both in terms of masses and in terms of mass ratios. Interestingly, the most massive event GW170729 (The LIGO Scientific Collaboration & the Virgo Collaboration 2018a) lies in a region that is populated only by merging exchanged BBHs.

Table 4 summarizes the masses of the most massive merging BBHs in our simulations (with $m_{\rm tot} \geq 70$ M$_\odot$). All of them are SC exchanged BBHs. The mass of the primary spans from 35 to 90 M$_\odot$, with five BHs more massive than 60 M$_\odot$ (these lie in the mass gap produced by PPISNe and PISNe). The mass of the secondary ranges from 24 to 48 M$_\odot$. These massive merging BBHs have median mass ratio $q = 0.75$, significantly lower than 1. The most massive binary ($m_1 = 90$ M$_\odot$, $m_2 = 31$ M$_\odot$) has also the lowest mass ratio $q = 0.34$.

3.3 Orbital eccentricity of merging BBHs

Orbital eccentricity is another feature which can be probed with current and future GW detectors (Nishizawa et al. 2016, 2017; Rodriguez et al. 2018). Dynamical exchanges tend to produce more eccentric binaries, although GW emission circularizes them very efficiently. Thus, even binaries with extreme eccentricity might achieve almost null eccentricity when they reach the LIGO–Virgo band (>10 Hz). However, a significant fraction of exchanged BBHs formed in SCs (e.g. Arca-Sedda et al. 2018; Rodriguez et al. 2018; Samsing 2018) or nuclear SCs (e.g. Antonini & Rasio 2016) is predicted to have eccentricity $e \gtrsim 10^{-2}$ when entering the LISA band ($\sim 10^{-4} - 1$ Hz).

Table 4. Heavy merging BBHs.

m_1 (M$_\odot$)	m_2 (M$_\odot$)	q
90	31	0.34
79	35	0.44
63	47	0.75
62	38	0.53
61	46	0.75
57	48	0.84
54	42	0.78
51	36	0.71
51	24	0.47
50	47	0.94
50	39	0.78
48	41	0.85
48	35	0.73
49	30	0.61
40	36	0.78
36	36	1.00
35	35	1.00

Note: Properties of merging BBHs with total mass $m_{\rm tot} \geq 70$ M$_\odot$. Column 1: primary mass (m_1); column 2: secondary mass (m_2); column 3: mass ratio (q). All these binaries are exchanged BBHs.

Fig. 9 shows the initial eccentricity $e_{\rm in}$ of our merging BBHs (i.e. the orbital eccentricity of the binary when it becomes a BBH binary) and the eccentricity $e_{\rm LISA}$ when the orbital frequency is $f_{\rm orb} = 10^{-2}$ Hz (approximately associated with the maximum sensitivity of LISA, see Amaro-Seoane et al. 2017). To estimate $e_{\rm LISA}$, we evolve the BBHs up to $f_{\rm orb} = 10^{-2}$ Hz following Peters (1964) equations.

The initial eccentricity distribution of SC merging exchanged BBHs shows an upturn for $e_{\rm in} > 0.6$ and is clearly different from both SC merging original BBHs and IBs. In contrast, when entering the LISA band, all systems (including exchanged BBHs) have significantly circularized. The minimum detectable eccentricity by LISA is $e_{\rm LISA} \sim 10^{-2}$, according to Nishizawa et al. (2016). Only $\sim$2.5 per cent ($\sim$1.6 per cent) merging exchanged BBHs (merging BBHs in IBs) have $e_{\rm LISA} \gtrsim 10^{-2}$.

Our results confirm that BBHs formed by exchange have significantly larger eccentricity at formation than other BBHs (see e.g. Ziosi et al. 2014). However, the maximum eccentricity of young SC BBHs in the LISA band is significantly smaller than the distribution of BBHs in both globular clusters and nuclear SCs (Nishizawa et al. 2016, 2017; Rodriguez et al. 2018).

3.4 Delay time distribution

A key quantity to predict the merger rate and the properties of merging BBHs is the delay time, i.e. the time elapsed between the formation of the stellar progenitors and the merger of the two BHs.

Fig. 10 shows that SC BBHs undergo a faster merger than BBHs in IBs. In particular, the distribution of delay times for SC merging BBHs scales as $dN/dt_{\rm delay} \propto t_{\rm delay}^{-1}$ while IB merging BBHs follow a shallower slope, with significantly less mergers in the first Gyr and a more populated tail with $t_{\rm delay} \gtrsim 5$ Gyr. This suggests that dynamical interactions in young SCs can speed up the merger of BBHs.

Furthermore, the delay time distribution of BBHs in our IB sample is significantly shallower than $\propto t_{\rm delay}^{-1}$, which is the slope found by Dominik et al. (2012) in their population-synthesis simulations. In IBs, the distribution of delay time depends on progenitor's metallicity, common envelope efficiency (described by α), and natal kicks (see Giacobbo & Mapelli 2018 for more details).

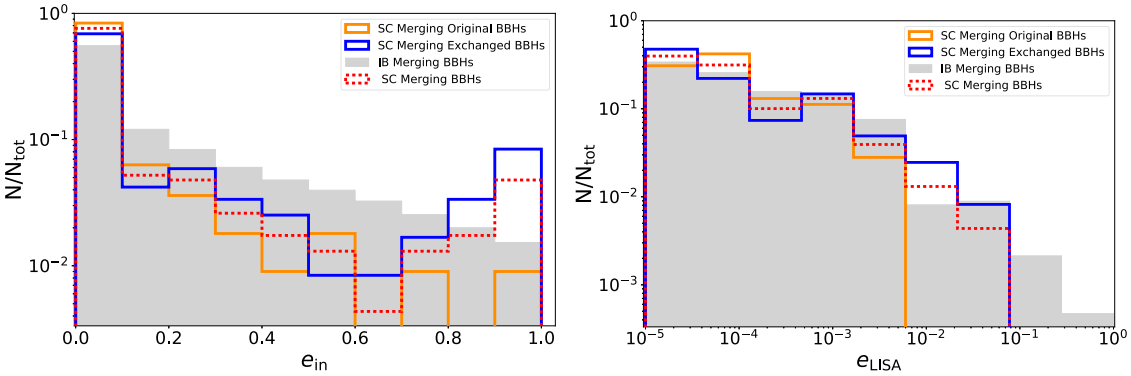

Figure 9. Distribution of eccentricities of merging BBHs in SCs and in IBs. All merging BBHs in SCs are shown by the dashed red line. BBHs in IBs are shown by the filled grey histogram. SC merging original BBHs and SC merging exchanged BBHs are shown with an orange and blue line, respectively. The eccentricity $e_{\rm in}$ (left) is calculated when the binary becomes a BBH, while $e_{\rm LISA}$ (right) is calculated when the orbital frequency is $f_{\rm orb} = 10^{-2}$ Hz (where the sensitivity of LISA is approximately maximum). In the right-hand panel, eccentricities $e_{\rm LISA}$ equal to zero have been set equal to 10^{-5}.

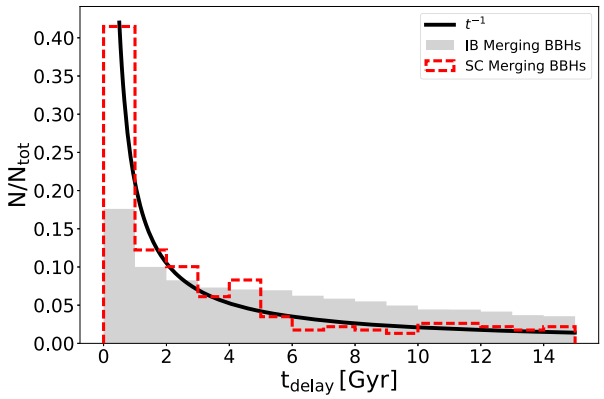

Figure 10. Distribution of the delay time-scales $t_{\rm delay}$ of merging BBHs. Grey shaded histogram: merging BBHs in IBs; red dashed line: all merging BBHs from SC simulations (exchanged BBHs plus original BBHs).

In particular, if we assume $\alpha \geq 3$ the fraction of BBHs with $t_{\rm delay} \leq 1$ Gyr is significantly reduced with respect to lower values of α (see fig. 6 of Giacobbo & Mapelli 2018). This explains why our merging BBHs in IBs (simulated with $\alpha = 3$) have a delay time distribution significantly flatter than that of Dominik et al. (2012), which assume $\alpha = 1$.

3.5 Number of mergers per unit stellar mass

Does SC dynamics boost the merger rate, too?

The simulations presented in this paper are not sufficient to estimate the merger rate, because we considered only one stellar metallicity and we know from previous papers (Giacobbo & Mapelli 2018) that the merger rate of BBHs is very sensitive to stellar metallicity. However, we can estimate the merger efficiency, i.e. the number of mergers per unit stellar mass for a given metallicity $N_m(Z)$, integrated over the Hubble time.

As detailed in Giacobbo et al. (2018), $N_m(Z)$ is the number of BBH mergers we find in the simulated sample ($N_{\rm merger}$), divided by the total initial mass of the stellar population (M_*):

$$N_m(Z) = \frac{N_{\rm merger}}{M_*}. \quad (8)$$

Table 5. Number of mergers per unit stellar mass.

Set	$N_m(Z = 0.002)$ ($M_\odot{}^{-1}$)
HF	1.75×10^{-5}
LF	1.61×10^{-5}
SC	1.68×10^{-5}
IB	1.70×10^{-5}

Note: Column 1: Name of the simulation set; column 2: $N_m(Z = 0.002)$ as defined in equation 8.

For the N-body simulations, M_* is just the total initial stellar mass of the simulated SCs, because the simulated SCs already include star masses ranging between 0.1 and 150 $M_\odot$ and because we use a quite realistic initial binary fraction ($f_{\rm bin} = 0.4$). In contrast, in the IB simulations, $M_* = M_{*,\rm sim}/(f_{\rm bin}\, f_{\rm corr})$, where $M_{*,\rm sim}$ is the total initial stellar mass of the simulated IBs, $f_{\rm bin} = 0.4$ accounts for the fact that we are simulating only binaries and not single stars, and $f_{\rm corr}$ accounts for the missing low-mass stars between 0.1 and 5 $M_\odot$ (see Table 1).

The values of $N_m(Z = 0.002)$ for the four simulation sets presented in this paper are shown in Table 5. The merger efficiency of the four simulation sets are remarkably similar. This implies that dynamics in young SCs does not affect the merger rate significantly.

Indeed, dynamics changes the properties of merging binaries (leading to the formation of more massive BBHs), but does not change their number significantly. The number of merging BBHs which form by exchange or harden by dynamical interactions appears to be compensated by the suppression of light merging BBHs (see Fig. 5). In a forthcoming study (Di Carlo et al., in preparation) we will check whether this result depends on stellar metallicity or on other properties of the simulated SCs.

3.6 Impact of fractality

So far, we have considered HF and LF simulations as a single simulation sample (SC simulations), because fractality does not significantly affect most of BBH properties (e.g. the number of merging BBHs, the merger efficiency, and the mass of merging BHs, see Table 3). Thus, we can conclude that the level of substructures does not significantly affect the merger of BBHs and can be neglected in future studies. This result is important because it

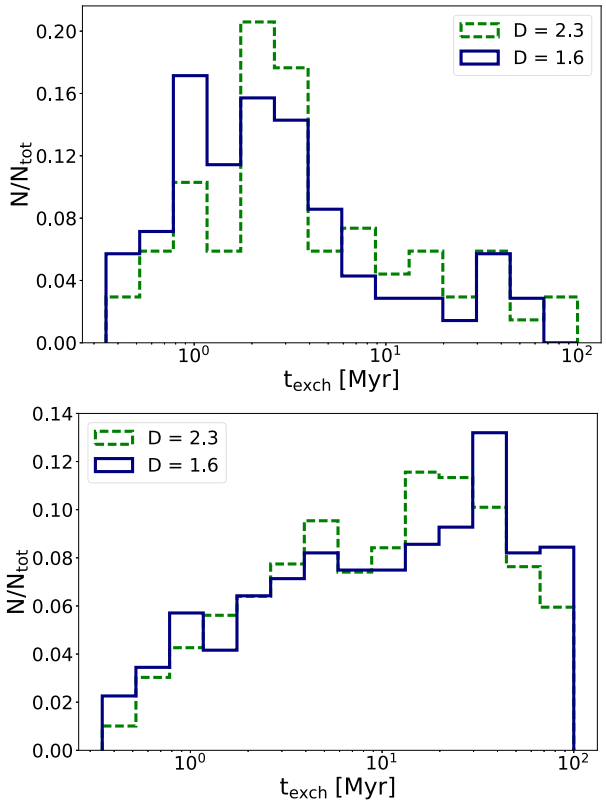

Figure 11. Formation times of merging exchanged BBHs (top panel) and of all exchanged BBHs (bottom). The formation time is defined as the time interval between the beginning of the simulation and the moment in which the binary forms. We show the distributions for fractal dimensions $D = 2.3$ (green dashed) and for $D = 1.6$ (blue solid). Each distribution is normalized to its total number of elements.

removes one of the possible parameters which were thought to affect the statistics of BBHs.

However, there are a couple of intriguing differences between HF and LF simulations (see Table 3), although these differences are only marginally significant.

First, the HF clusters tend to produce merging BBHs with larger mass ratios than the LF clusters (median values of $q = 0.9$ and $q = 0.8$ in HF and LF simulations, respectively, see Table 3). Secondly, the median time of dynamical exchange for merging exchanged BBHs ($t_{\rm exch}$, i.e. the time when a dynamical exchange leads to the formation of the binary which then becomes a merging BBH) is $t_{\rm exch} = 1.9$ and 2.8 Myr for HF and LF clusters, respectively (see also Fig. 11).

Although only marginally significant, these differences are consistent with our expectations. In fact, the more fractal (i.e. substructured) an SC is, the shorter is its two-body relaxation time-scale $t_{\rm rlx}$ (see e.g. Fujii & Portegies Zwart 2014). A shorter two-body relaxation time-scale implies also a shorter core-collapse time-scale. Core collapse is the moment of the life of an SC when three-body encounters and exchanges are more likely to occur, because of the boost in the central density. Thus, we expect dynamical exchanges (leading to the formation of merging BBHs) to occur earlier in HF simulations than in LF simulations.

Moreover, if $t_{\rm exch} < 3$ Myr, the exchange occurs before the binary has turned into a BBH, because the lifetime of the most massive stars is $\gtrsim 3$ Myr. If the binary which forms after an exchange is still composed of two non-degenerate stars (or a star and a BH), it may still undergo mass transfer and common envelope after the exchange. This mass transfer or common envelope is expected to 'redistribute' the mass between the two members of the binary, leading to the formation of an almost equal mass BBH. In contrast, if $t_{\rm exch} \gg 3$ Myr, the outcome of the exchange is already a BBH, which cannot undergo mass transfer and whose mass ratio can be small. For this reason, the fact that $t_{\rm exch}$ is significantly shorter in HF clusters than in LF clusters implies that the median q of the former is larger than the median q of the latter, because exchanged binaries in HF clusters have more chances to undergo common envelope than exchanged binaries in LF clusters.

4 COMPARISON WITH PREVIOUS WORK

Our BH mass spectrum (Fig. 3) is significantly different from the one reported by previous papers on BBHs in young SCs. In comparison with the BH mass spectrum reported by Banerjee (2018) and Banerjee et al. (2019), our mass spectrum is broader, we form more massive BHs and our distribution peaks at a lower mass value (see fig. 1 of Banerjee 2018 and our Fig. 3). As a result, we form merging BBHs with both lower and higher total masses. This is a consequence of our different wind mass-loss and SN prescriptions. Furthermore, we find significantly smaller eccentricities in the LISA band ($e_{\rm LISA}$); this could depend on post-Newtonian terms, which are not included in our study and are taken into account in Banerjee (2018). Similarly, Rastello et al. (2019) find only very eccentric merging BBHs ($e \geq 0.99$), while most of our merging BBHs have a nearly circular orbit.

In contrast, the eccentricity (Fig. 9) and delay time distribution (Fig. 10) of merging BBHs in our simulations are in good agreement with Kumamoto et al. (2019). Similar to Kumamoto et al. (2019), we find that most exchanged merging BBHs undergo the first exchange before the second BH has formed: these systems undergo a common envelope after the first exchange.

Another parameter that may affect the statistics of BBHs is the initial binary fraction $f_{\rm bin}$. We assume $f_{\rm bin} = 0.4$, while observations seem to indicate $f_{\rm bin} \sim 0.6$–0.7 (Sana et al. 2012). We stress that $f_{\rm bin} = 0.4$ is the highest initial binary fraction ever assumed in a large set of direct N-body simulations studying BBHs, because the number of initial binaries is the bottleneck of direct N-body simulations. Indeed, most previous studies of BBHs in young SCs assume no initial binaries (e.g. Banerjee et al. 2010; Mapelli 2016; Banerjee 2017; Kumamoto et al. 2019) or lower values of $f_{\rm bin}$ (e.g. $f_{\rm bin} = 0.2$ in Ziosi et al. 2014). Assuming a higher value of $f_{\rm bin}$ would likely affect the number of original BBHs only: Mapelli & Zampieri (2014) find that the number of original BH binaries grows almost linearly with $f_{\rm bin}$, while the number of exchanged BH binaries remains almost unchanged.

5 DISCUSSION

We have shown that young SC dynamics crucially affects the main properties (mass, eccentricity, and delay time) of merging BBHs, but how common is the dynamical formation of BBHs in young SCs?

Star formation (and especially massive star formation) is expected to occur mostly in young SCs and associations (Lada & Lada 2003; Portegies Zwart et al. 2010). This implies that most BBH progenitors were born in SCs or OB associations, and a significant fraction of them underwent dynamical interactions before being ejected from their parent SC, or before the SC dissolved in the galactic tidal field.

Is the time spent by a BBH (or BBH progenitor) in the parent SC sufficient to significantly affect the properties of merging BBHs?

The crucial point is to understand when merging exchanged BBHs form in our simulations. In fact, our simulations include a static tidal field, assuming that the simulated SCs are on circular orbits approximately at the location of the Sun. This approach tends to overestimate the lifetime of SCs, because we do not account for orbits closer to the galactic centre and, most importantly, we do not account for massive perturbers (e.g. molecular clouds), which might accelerate the disruption of the parent SC (Gieles et al. 2006).

Fig. 11 shows the time of the dynamical exchange for merging exchanged BBHs (top) and for all exchanged BBHs (bottom). While most exchanged BBHs form at late stages in the evolution of their parent SC, the majority of merging exchanged BBHs form in the first ∼10 Myr. This guarantees that the majority of merging exchanged BBHs would have formed even if the tidal field was locally stronger.

The difference between top and bottom panel of Fig. 11 can be explained straightforwardly with the nature of the exchanged binaries: only ∼13 per cent of merging exchanged BBHs originate from a dynamical exchange which leads to the immediate formation of a BBH, while the dynamical exchange produces a new star–star binary (i.e. a binary system composed of two stars) and a BH–star binary in the ∼77 per cent and 10 per cent of systems, respectively. In contrast, ∼59 per cent of all exchanged BBHs form from dynamical exchanges which lead to the formation of a BBH directly, while 37 per cent (4 per cent) exchanges produce star–star (BH–star) binaries. This implies that binaries which undergo an exchange before both stars have turned into BHs are more likely to merge within a Hubble time. The reason is that exchanged star–star binaries and BH–star binaries can still undergo common envelope episodes, which shrink their orbital separation significantly and favour their merger within a Hubble time. Thus, in young SCs, stellar binary evolution and dynamics strictly cooperate to the formation of merging exchanged BBHs.

In contrast, double degenerate binaries can shrink only by three-body encounters and by GW decay, which are not as efficient as common envelope. Thus, most exchanged BBHs which form at late times cannot merge within a Hubble time. In this regard, young SCs are quite different from globular clusters (Rodriguez et al. 2015; Rodriguez et al. 2016; Askar et al. 2017): a large fraction of exchanged BBHs in globular clusters remain inside the parent SCs for many Gyr, undergoing several exchanges and shrinking efficiently by dynamical hardening, while most exchanged binaries in young SCs undergo a single exchange and harden for a short time span.

In this work, we have chosen to stop the integration of our SCs 100 Myr after their formation. A possible issue connected with this choice is whether dynamical exchanges and hardening might have played a role even after 100 Myr. According to Gieles et al. (2006), the estimated lifetime of an SC with mass 10^4 $M_\odot$ in the solar neighbourhood is ∼1 Gyr. Only $\lesssim 6$ per cent of our simulated SCs have mass $M_{SC} \geq 10^4$ $M_\odot$, while most of them have a mass of $\sim 10^3$ $M_\odot$. Thus, their lifetime is $<<1$ Gyr. Moreover, we expect that dynamics does not affect much the statistics of merging BBHs after 100 Myr, because we find that on average only ∼0.23 BBHs and ∼0.41 single BHs per SC are still inside their parent SC at the end of the simulations.

A further crucial question is whether there are unique signatures of merging exchanged BBHs, which can be chased by GW detectors. The masses of merging BBHs formed via SC and IB simulations are remarkably different in our simulations. However, lower progenitor metallicity can induce the formation of more massive merging BBHs in IBs (e.g. Giacobbo & Mapelli 2018). Thus, the effects of metallicity and dynamics are somewhat degenerate.

On the other hand, the most straightforward smoking gun of dynamical evolution is the formation of merging BHs in the mass range forbidden by (pulsational) pair instability (≈60–120 $M_\odot$, Spera & Mapelli 2017). In our dynamical simulations, only 5 out of 229 merging BBHs (∼2 per cent of all merging BBHs) fall in this forbidden mass range. Currently, no GW events lie in this mass range, but the detection of one such BBHs would be a strong support for the dynamical formation channel. In a forthcoming study, we will generalize our results to different stellar metallicities.

6 SUMMARY

We have investigated the formation of BBHs in young SCs and open clusters. These SCs represent the bulk of star formation in galaxies. For our study, we have integrated the new population synthesis code MOBSE, which implements up-to-date stellar winds, binary evolution, and SN models (Mapelli et al. 2017; Giacobbo et al. 2018; Giacobbo & Mapelli 2018), with the direct summation N-body code NBODY6++GPU, which allows us to account for close encounters and dynamical exchanges (Wang et al. 2015).

We find that dynamics significantly affects the properties of merging BBHs: dynamical exchanges favour the formation and the merger of massive BBHs with total mass up to $m_{tot} \sim 120$ $M_\odot$ and with mass ratio ranging from $q \sim 1$ to $q \sim 0.1$ (although large mass ratios are more likely).

For comparison, merging BBHs evolved in IBs (run with the same population synthesis code) have maximum total mass $m_{tot} \lesssim 70$ $M_\odot$ and a significantly stronger preference for large mass ratios.

The masses of merging BBHs in our simulations are consistent with the first 10 BBHs observed by the LIGO–Virgo collaboration (The LIGO Scientific Collaboration & the Virgo Collaboration 2018a, b). At the simulated metallicity ($Z = 0.002$), the BH mass of GW170729 ($m_1 = 50.6^{+16.6}_{-10.2}$, $m_2 = 34.4^{+9.1}_{-10.1}$ $M_\odot$, The LIGO Scientific Collaboration & the Virgo Collaboration 2018a) can be matched only by dynamically formed BBHs, within the 90 per cent credible interval.

On the other hand, young SC dynamics does not affect the merger rate. We find almost the same merger efficiency ($\mathcal{N}_m \sim 1.7 \times 10^{-5}$ $M_\odot^{-1}$) in SC and in IB simulations. The formation of massive merging BBHs by dynamical exchanges is compensated by the loss of light merging BBHs, which are softened or ionized by interactions.

Almost all BBHs in our simulations merge after they were ejected from the SC or after the SC dissolved and became field.

Dynamics tends to speed up the merger of BBHs: the delay time between the formation of the stellar progenitors and the merger of the BBH scales approximately as $dN/dt_{delay} \propto t_{delay}^{-1}$ for SC merging BBHs, while the trend is shallower for IB merging BBHs.

Finally, about 2 per cent of merging BHs formed in young SCs have mass $\gtrsim 60$ $M_\odot$, lying in the 'forbidden' region by (pulsational) pair instability ($m_{BH} \sim$ 60–120 $M_\odot$, e.g. Spera & Mapelli 2017). These BHs form by the merger of two or more stars. According to our prescriptions, merged metal-poor stars with a Helium core smaller than ∼60 $M_\odot$ might retain a large hydrogen envelope: they avoid the pair-instability SN window and might collapse to massive BHs. In the field, such massive BHs remain single, while in young SCs they can acquire companions dynamically and merge by GW emission. Thus, observing a rare merging BBH with mass $\gtrsim 60$ $M_\odot$ would be a strong signature of dynamical formation.

ACKNOWLEDGEMENTS

We thank the referee Manuel Arca-Sedda for his careful reading of the manuscript and for his many useful suggestions. We thank all the members of the ForDyS group for their useful comments. We thank Sambaran Banerjee, Mirek Giersz, and Abbas Askar for the useful discussions. UNDC acknowledges financial support from Università degli Studi dell'Insubria through a Cycle 33rd PhD grant. MM acknowledges financial support by the European Research Council for the ERC Consolidator grant DEMOBLACK, under contract no. 770017. MP acknowledges financial support from the European Union's Horizon 2020 research and innovation programme under the Marie Sklodowska-Curie grant agreement No. 664931. MS acknowledges funding from the European Union's Horizon 2020 research and innovation programme under the Marie-Sklodowska-Curie grant agreement No. 794393. LW acknowledges financial support from Alexander von Humboldt Foundation. This work benefited from support by the International Space Science Institute (ISSI), Bern, Switzerland, through its International Team programme ref. no. 393 *The Evolution of Rich Stellar Populations & BH Binaries* (2017-18).

REFERENCES

Aarseth S. J., 2003, Gravitational N-Body Simulations, Cambridge Univ. Press
Aasi J. et al., 2015, Class. Quantum Gravity, 32, 074001
Abbott B. P. et al., 2016a, Phys. Rev. X, 6, 041015
Abbott B. P. et al., 2016b, Phys. Rev. Lett., 116, 061102
Abbott B. P. et al., 2016c, Phys. Rev. Lett., 116, 241103
Abbott B. P. et al., 2016d, ApJ, 818, L22
Abbott B. P. et al., 2017a, Phys. Rev. Lett., 118, 221101
Abbott B. P. et al., 2017b, Phys. Rev. Lett., 119, 141101
Abbott B. P. et al., 2017c, Phys. Rev. Lett., 119, 161101
Abbott B. P. et al., 2017d, ApJ, 848, L12
Abbott B. P. et al., 2017e, ApJ, 848, L13
Abbott B. P. et al., 2017f, ApJ, 851, L35
Acernese F. et al., 2015, Class. Quantum Gravity, 32, 024001
Alexander K. D. et al., 2017, ApJ, 848, L21
Amaro-Seoane P. et al., 2017, preprint (arXiv:1702.00786)
Antonini F., Rasio F. A., 2016, ApJ, 831, 187
Antonini F., Chatterjee S., Rodriguez C. L., Morscher M., Pattabiraman B., Kalogera V., Rasio F. A., 2016, ApJ, 816, 65
Antonini F., Gieles M., Gualandris A., 2019, MNRAS, 486, 5008
Arca-Sedda M., Gualandris A., 2018, MNRAS, 477, 4423
Arca-Sedda M., Li G., Kocsis B., 2018, preprint (arXiv:1805.06458)
Askar A., Szkudlarek M., Gondek-Rosińska D., Giersz M., Bulik T., 2017, MNRAS, 464, L36
Askar A., Arca Sedda M., Giersz M., 2018, MNRAS, 478, 1844
Banerjee S., 2017, MNRAS, 467, 524
Banerjee S., 2018, MNRAS, 473, 909
Banerjee S., Baumgardt H., Kroupa P., 2010, MNRAS, 402, 371
Banerjee S., Belczynski K., Fryer C. L., Berczik P., Hurley J. R., Spurzem R., Wang L., 2019, preprint (arXiv:1902.07718)
Bauer D. F., 1972, J. Am. Stat. Assoc., 67, 687
Belczynski K., Kalogera V., Bulik T., 2002, ApJ, 572, 407
Belczynski K., Taam R. E., Kalogera V., Rasio F. A., Bulik T., 2007, ApJ, 662, 504
Belczynski K., Kalogera V., Rasio F. A., Taam R. E., Zezas A., Bulik T., Maccarone T. J., Ivanova N., 2008, ApJS, 174, 223
Belczynski K., Bulik T., Fryer C. L., Ruiter A., Valsecchi F., Vink J. S., Hurley J. R., 2010, ApJ, 714, 1217
Belczynski K., Holz D. E., Bulik T., O'Shaughnessy R., 2016a, Nature, 534, 512
Belczynski K. et al., 2016b, A&A, 594, A97
Bethe H. A., Brown G. E., 1998, ApJ, 506, 780
Birnbaum Z., Tingey F. H., 1951, Ann. Math. Stat., 22, 592
Carr B., Kühnel F., Sandstad M., 2016, Phys. Rev. D, 94, 083504
Cartwright A., Whitworth A. P., 2004, MNRAS, 348, 589
Chatterjee S., Rodriguez C. L., Kalogera V., Rasio F. A., 2017, ApJ, 836, L26
Chen Y., Bressan A., Girardi L., Marigo P., Kong X., Lanza A., 2015, MNRAS, 452, 1068
Chornock R. et al., 2017, ApJ, 848, L19
Chruslinska M., Belczynski K., Klencki J., Benacquista M., 2018, MNRAS, 474, 2937
Claeys J. S. W., Pols O. R., Izzard R. G., Vink J., Verbunt F. W. M., 2014, A&A, 563, A83
Colpi M., Mapelli M., Possenti A., 2003, ApJ, 599, 1260
Coulter D. A. et al., 2017, Science, 358, 1556
Cowperthwaite P. S. et al., 2017, ApJ, 848, L17
de Mink S. E., Mandel I., 2016, MNRAS, 460, 3545
Dessart L., Burrows A., Ott C. D., Livne E., Yoon S.-C., Langer N., 2006, ApJ, 644, 1063
Dominik M., Belczynski K., Fryer C., Holz D. E., Berti E., Bulik T., Mandel I., O'Shaughnessy R., 2012, ApJ, 759, 52
Dominik M., Belczynski K., Fryer C., Holz D. E., Berti E., Bulik T., Mandel I., O'Shaughnessy R., 2013, ApJ, 779, 72
Dominik M. et al., 2015, ApJ, 806, 263
Downing J. M. B., Benacquista M. J., Giersz M., Spurzem R., 2010, MNRAS, 407, 1946
Downing J. M. B., Benacquista M. J., Giersz M., Spurzem R., 2011, MNRAS, 416, 133
Eldridge J. J., Stanway E. R., Tang P. N., 2019, MNRAS, 482, 870
Elmegreen B. G., Efremov Y. N., 1997, ApJ, 480, 235
Farr W. M., Sravan N., Cantrell A., Kreidberg L., Bailyn C. D., Mandel I., Kalogera V., 2011, ApJ, 741, 103
Flannery B. P., van den Heuvel E. P. J., 1975, A&A, 39, 61
Fryer C. L., Belczynski K., Wiktorowicz G., Dominik M., Kalogera V., Holz D. E., 2012, ApJ, 749, 91
Fujii M. S., Portegies Zwart S., 2014, MNRAS, 439, 1003
Fujii M. S., Tanikawa A., Makino J., 2017, PASJ, 69, 94
Gerosa D., Berti E., 2017, Phys. Rev. D, 95, 124046
Giacobbo N., Mapelli M., 2018, MNRAS, 480, 2011
Giacobbo N., Mapelli M., 2019, MNRAS, 482, 2234
Giacobbo N., Mapelli M., Spera M., 2018, MNRAS, 474, 2959
Gieles M., Portegies Zwart S. F., Baumgardt H., Athanassoula E., Lamers H. J. G. L. M., Sipior M., Leenaarts J., 2006, MNRAS, 371, 793
Giersz M., Leigh N., Hypki A., Lützgendorf N., Askar A., 2015, MNRAS, 454, 3150
Goldstein A. et al., 2017, ApJ, 848, L14
Goodman J., Hut P., 1993, ApJ, 403, 271
Goodwin S. P., Whitworth A. P., 2004, A&A, 413, 929
Goswami S., Kiel P., Rasio F. A., 2014, ApJ, 781, 81
Gräfener G., Hamann W.-R., 2008, A&A, 482, 945
Gürkan M. A., Fregeau J. M., Rasio F. A., 2006, ApJ, 640, L39
Gutermuth R. A., Megeath S. T., Pipher J. L., Williams J. P., Allen L. E., Myers P. C., Raines S. N., 2005, ApJ, 632, 397
Heger A., Fryer C. L., Woosley S. E., Langer N., Hartmann D. H., 2003, ApJ, 591, 288
Heggie D. C., 1975, MNRAS, 173, 729
Hills J. G., Fullerton L. W., 1980, AJ, 85, 1281
Hoang B.-M., Naoz S., Kocsis B., Rasio F. A., Dosopoulou F., 2018, ApJ, 856, 140
Hobbs G., Lorimer D. R., Lyne A. G., Kramer M., 2005, MNRAS, 360, 974
Hollander M., Wolfe D. A., 1999, Nonparametric Statistical Methods, 2 edn. Wiley-Interscience, Hoboken, NJ
Hurley J. R., Pols O. R., Tout C. A., 2000, MNRAS, 315, 543
Hurley J. R., Tout C. A., Pols O. R., 2002, MNRAS, 329, 897
Hurley J. R., Sippel A. C., Tout C. A., Aarseth S. J., 2016, Publ. Astron. Soc. Aust., 33, e036
Jones S. et al., 2013, ApJ, 772, 150
Kimpson T. O., Spera M., Mapelli M., Ziosi B. M., 2016, MNRAS, 463, 2443

King I. R., 1966, AJ, 71, 64
Kouwenhoven M. B. N., Goodwin S. P., Parker R. J., Davies M. B., Malmberg D., Kroupa P., 2010, MNRAS, 404, 1835
Kozai Y., 1962, AJ, 67, 591
Kroupa P., 2001, MNRAS, 322, 231
Kroupa P., Boily C. M., 2002, MNRAS, 336, 1188
Kruckow M. U., Tauris T. M., Langer N., Kramer M., Izzard R. G., 2018, MNRAS, 481, 1908
Kulkarni S. R., Hut P., McMillan S., 1993, Nature, 364, 421
Kumamoto J., Fujii M. S., Tanikawa A., 2019, MNRAS, 486, 3942
Küpper A. H. W., Maschberger T., Kroupa P., Baumgardt H., 2011, MNRAS, 417, 2300
Lada C. J., Lada E. A., 2003, ARA&A, 41, 57
Lidov M. L., 1962, Planet. Space Sci., 9, 719
Makino J., Aarseth S. J., 1992, PASJ, 44, 141
Mapelli M., 2016, MNRAS, 459, 3432
Mapelli M., 2018, preprint (arXiv:1809.09130)
Mapelli M., Bressan A., 2013, MNRAS, 430, 3120
Mapelli M., Zampieri L., 2014, ApJ, 794, 7
Mapelli M., Giacobbo N., 2018, MNRAS, 479, 4391
Mapelli M., Colpi M., Zampieri L., 2009, MNRAS, 395, L71
Mapelli M., Ripamonti E., Zampieri L., Colpi M., Bressan A., 2010, MNRAS, 408, 234
Mapelli M., Zampieri L., Ripamonti E., Bressan A., 2013, MNRAS, 429, 2298
Mapelli M., Giacobbo N., Ripamonti E., Spera M., 2017, MNRAS, 472, 2422
Mapelli M., Giacobbo N., Toffano M., Ripamonti E., Bressan A., Spera M., Branchesi M., 2018, MNRAS, 481, 5324
Mapelli M., Giacobbo N., Santoliquido F., Artale M. C., 2019, MNRAS, 487, 2
Marchant P., Langer N., Podsiadlowski P., Tauris T. M., Moriya T. J., 2016, A&A, 588, A50
Margutti R. et al., 2017, ApJ, 848, L20
Marks M., Kroupa P., Dabringhausen J., Pawlowski M. S., 2012, MNRAS, 422, 2246
Mennekens N., Vanbeveren D., 2014, A&A, 564, A134
Miller M. C., Hamilton D. P., 2002, MNRAS, 330, 232
Miller M. C., Lauburg V. M., 2009, ApJ, 692, 917
Moody K., Sigurdsson S., 2009, ApJ, 690, 1370
Nicholl M. et al., 2017, ApJ, 848, L18
Nishizawa A., Berti E., Klein A., Sesana A., 2016, Phys. Rev. D, 94, 064020
Nishizawa A., Sesana A., Berti E., Klein A., 2017, MNRAS, 465, 4375
Nitadori K., Aarseth S. J., 2012, MNRAS, 424, 545
O'Leary R. M., Rasio F. A., Fregeau J. M., Ivanova N., O'Shaughnessy R., 2006, ApJ, 637, 937
O'Leary R. M., Kocsis B., Loeb A., 2009, MNRAS, 395, 2127
O'Leary R. M., Meiron Y., Kocsis B., 2016, ApJ, 824, L12
Orosz J. A., 2003, in van der Hucht K., Herrero A., Esteban C., eds, Proc. IAU Symp. 212, A Massive Star Odyssey: From Main Sequence to Supernova. Kluwer, Dordrecht, p. 365
Özel F., Psaltis D., Narayan R., McClintock J. E., 2010, ApJ, 725, 1918
Peters P. C., 1964, Phys. Rev., 136, 1224
Pian E. et al., 2017, Nature, 551, 67
Podsiadlowski P., Langer N., Poelarends A. J. T., Rappaport S., Heger A., Pfahl E., 2004, ApJ, 612, 1044
Podsiadlowski P., Dewi J. D. M., Lesaffre P., Miller J. C., Newton W. G., Stone J. R., 2005, MNRAS, 361, 1243
Portegies Zwart S. F., 2016, MNRAS, 457, 313
Portegies Zwart S. F., Yungelson L. R., 1998, A&A, 332, 173
Portegies Zwart S. F., McMillan S. L. W., 2000, ApJ, 528, L17
Portegies Zwart S. F., McMillan S. L. W., 2002, ApJ, 576, 899
Portegies Zwart S. F., Baumgardt H., Hut P., Makino J., McMillan S. L. W., 2004, Nature, 428, 724
Portegies Zwart S. F., McMillan S. L. W., Gieles M., 2010, ARA&A, 48, 431
Raccanelli A., Kovetz E. D., Bird S., Cholis I., Muñoz J. B., 2016, Phys. Rev. D, 94, 023516
Rastello S., Amaro-Seoane P., Arca-Sedda M., Capuzzo-Dolcetta R., Fragione G., Tosta e Melo I., 2019, MNRAS, 483, 1233
Rodriguez C. L., Morscher M., Pattabiraman B., Chatterjee S., Haster C.-J., Rasio F. A., 2015, Phys. Rev. Lett., 115, 051101
Rodriguez C. L., Chatterjee S., Rasio F. A., 2016, Phys. Rev. D, 93, 084029
Rodriguez C. L., Amaro-Seoane P., Chatterjee S., Kremer K., Rasio F. A., Samsing J., Ye C. S., Zevin M., 2018, Phys. Rev. D, 98, 123005
Sadowski A., Belczynski K., Bulik T., Ivanova N., Rasio F. A., O'Shaughnessy R., 2008, ApJ, 676, 1162
Samsing J., 2018, Phys. Rev. D, 97, 103014
Samsing J., D'Orazio D. J., 2018, MNRAS, 481, 5445
Samsing J., MacLeod M., Ramirez-Ruiz E., 2017, ApJ, 846, 36
Samsing J., Askar A., Giersz M., 2018, ApJ, 855, 124
Sana H. et al., 2012, Science, 337, 444
Sasaki M., Suyama T., Tanaka T., Yokoyama S., 2016, Phys. Rev. Lett., 117, 061101
Savchenko V. et al., 2017, ApJ, 848, L15
Scelfo G., Bellomo N., Raccanelli A., Matarrese S., Verde L., 2018, J. Cosmol. Astropart. Phys., 9, 039
Schwab J., Quataert E., Bildsten L., 2015, MNRAS, 453, 1910
Shao Y., Li X.-D., 2018, MNRAS, 477, L128
Sigurdsson S., Hernquist L., 1993, Nature, 364, 423
Sigurdsson S., Phinney E. S., 1995, ApJS, 99, 609
Soares-Santos M. et al., 2017, ApJ, 848, L16
Spera M., Mapelli M., 2017, MNRAS, 470, 4739
Spera M., Mapelli M., Bressan A., 2015, MNRAS, 451, 4086
Spera M., Mapelli M., Giacobbo N., Trani A. A., Bressan A., Costa G., 2019, MNRAS, 485, 889
Spitzer Jr. L., 1969, ApJ, 158, L139
Stiefel E., 1965, J. Reine Angew. Math., 218, 204
Tauris T. M., Langer N., Podsiadlowski P., 2015, MNRAS, 451, 2123
Tauris T. M. et al., 2017, ApJ, 846, 170
The LIGO Scientific Collaboration, the Virgo Collaboration, 2018a, preprint (arXiv:1811.12907)
The LIGO Scientific Collaboration, The Virgo Collaboration, 2018b, preprint (arXiv:1811.12940)
Trani A. A., Mapelli M., Bressan A., 2014, MNRAS, 445, 1967
Tutukov A., Yungelson L., 1973, Nauchnye Inf., 27, 70
VanLandingham J. H., Miller M. C., Hamilton D. P., Richardson D. C., 2016, ApJ, 828, 77
Vink J. S., 2017, Phil. Trans. R. Soc. A, 375, 20160269
Vink J. S., de Koter A., Lamers H. J. G. L. M., 2001, A&A, 369, 574
Vink J. S., Muijres L. E., Anthonisse B., de Koter A., Gräfener G., Langer N., 2011, A&A, 531, A132
Voss R., Tauris T. M., 2003, MNRAS, 342, 1169
Wang J., Tsang W. W., Marsaglia G., 2003, J. Stat. Softw., 8,
Wang L., Spurzem R., Aarseth S., Nitadori K., Berczik P., Kouwenhoven M. B. N., Naab T., 2015, MNRAS, 450, 4070
Wang L. et al., 2016, MNRAS, 458, 1450
Woosley S. E., 2017, ApJ, 836, 244
Zevin M., Pankow C., Rodriguez C. L., Sampson L., Chase E., Kalogera V., Rasio F. A., 2017, ApJ, 846, 82
Zevin M., Samsing J., Rodriguez C., Haster C.-J., Ramirez-Ruiz E., 2019, ApJ, 871, 91
Ziosi B. M., Mapelli M., Branchesi M., Tormen G., 2014, MNRAS, 441, 3703

This paper has been typeset from a TEX/LATEX file prepared by the author.